Bulletin of Pure and Applied Sciences
Geology, Vol.45F, No.2,
July-December 2026: P.45-58
Original Article

Print version ISSN 0970 4639
Online version ISSN 2320 3234

Available online at www.bpasjournals.com

ASSESSING PHYSICOCHEMICAL CONDITIONS OF PALEOCENE-EOCENE SYENITIC ROCKS IN THE CENTRAL SANANDAJ-SIRJAN ZONE, NORTH OF GOLPAYEGAN, IRAN

Somayeh Falahaty*

Author's Affiliations: PhD in Petrology/ Geology, University of Isfahan, Isfahan, Iran

***Corresponding Author: Somayeh Falahaty,** PhD in Petrology/ Geology, University of Isfahan, Isfahan, Iran
E-mail: somayehfalahaty2013@gmail.com, somayehfalahaty@yahoo.com

Received on 24.08.2026, Revised on 14.09.2026, Accepted on 31.10.2026

How to cite this article: Falahaty S. (2026). Assessing Physicochemical Conditions of Paleocene-Eocene Syenitic Rocks in the Central Sanandaj-Sirjan Zone, North of Golpayegan, Iran. *Bulletin of Pure and Applied Sciences- Geology,* 45F (2), 45-58.

Abstract:
The Sanandaj-Sirjan Zone (SSZ) records protracted subduction of the Arabian plate beneath Eurasia. This research examines syenitic plutonic rocks from the northern Golpayegan region, central SSZ, aiming to determine their crystallization conditions and tectonic setting. The rocks consist mainly of orthoclase, calcic amphibole (ferro-tschermakite), and biotite (lepidomelane), with biotite chemistry indicating crystallization from a potassic alkaline series, supported by whole-rock geochemistry. Amphibole-only thermobarometry (Ridolfi et al., 2010) yields crystallization temperatures of 882–915 °C (avg. 902 °C) and pressures of 3.68–5.59 kbar (avg. 4.67 kbar), corresponding to depths of ~15–18 km. Oxygen fugacity estimates, derived from biotite Fe^{3+}/Fe^{2+} ratios, yield a log fO_2 of approximately -13, indicating reducing conditions near the FMQ buffer. The alkaline affinity, mid-crustal emplacement, and reduced redox state, when combined with regional tectonic frameworks, point to a post-collisional origin linked to extensional fracturing after the Laramide orogenic pulse. These results provide quantitative P–T–fO_2 constraints on Paleocene-Eocene alkaline magmatism in this segment of the SSZ and are discussed within the broader context of regional tectonomagmatic evolution.

Keywords: *Syenitic rocks, Mineral chemistry, Geothermobarometer, Post-collisional magmatism, Sanandaj-Sirjan zone.*

1. INTRODUCTION

The northeastward subduction of the Southern Neotethyan oceanic lithosphere beneath the Eurasian plate, active from the Jurassic to the Cenozoic, resulted in the formation of two subduction-related magmatic arcs parallel to the Main Zagros Thrust: the Mesozoic Sanandaj-Sirjan Zone (SSZ) and the Cenozoic Urumieh-Dokhtar Magmatic Arc (Berberian and King, 1981; Moritz et al., 2006; Agard et al., 2005). However, recent studies have also proposed continental rifting as an alternative mechanism for some magmatic episodes in the SSZ (e.g., Nouri et al., 2023). The timing of arc magmatism in the SSZ was diachronous, initiating in the latest Triassic–Early Jurassic, peaking around 170 Ma, and terminating during the Late Cretaceous to Paleogene, with a northeastward shift to the Urumieh-Dokhtar arc. Eocene magmatic rocks in the SSZ are not necessarily granitic or shoshonitic in composition and should be viewed in the context of the regional Eocene magmatic flare-up documented across Iran (Verdel et al., 2011; Hassanzadeh and Wernicke, 2016).

The main scientific objective of this study is to address a key unanswered question regarding the syenitic rocks of northern Golpayegan: What were the physicochemical conditions (temperature, pressure, and oxygen fugacity) and tectonic setting of the parental magma? While previous studies have described the general geology and petrography of these rocks (e.g., Sharifi, 2007), no quantitative estimates of crystallization conditions have been provided. This study aims to fill this gap

by applying amphibole and biotite mineral chemistry as proxies for P–T–fO_2 conditions.

The compositions of index minerals such as amphibole and biotite are effective indicators of the physicochemical conditions of magma crystallization (e.g., Abdel-Rahman, 1994; Anderson and Smith, 1995). Amphibole is particularly reliable for estimating crystallization pressure and temperature (e.g., Hammarstrom and Zen, 1986; Schmidt, 1992; Ridolfi et al., 2010), while biotite, sensitive to redox changes, is valuable for estimating oxygen fugacity, although its use alone has limitations and should be supported by independent redox indicators (Wones and Eugster, 1965). This study presents new mineral chemistry data to reconstruct the P–T–fO_2 conditions of the Golpayegan syenitic magma and additionally evaluates its regional tectonic setting.

2. GEOLOGICAL SETTING

The Zagros fold-thrust belt formed as a result of the collision between the Arabian plate and the Iranian microcontinent following the closure of the Neo-Tethys Ocean during the Cenozoic (Agard et al., 2005; Pirouz et al., 2017). This orogenic system comprises three parallel belts: the Urumieh-Dokhtar Magmatic Belt, the Sanandaj-Sirjan Zone (SSZ), and the Zagros fold-thrust belt, along with the Persian Gulf Foreland Basin (Fig. 1; Agard et al., 2005). The SSZ represents an active Andean-like margin characterized by calc-alkaline magmatism and medium- to high-pressure metamorphism from the Middle Jurassic to the Late Cretaceous, related to northeastward subduction of the Neotethyan oceanic lithosphere (Berberian and King, 1981; Moritz et al., 2006; Pirouz et al., 2017).

The study area is located in the central part of the SSZ, near the city of Golpayegan (Fig. 1).

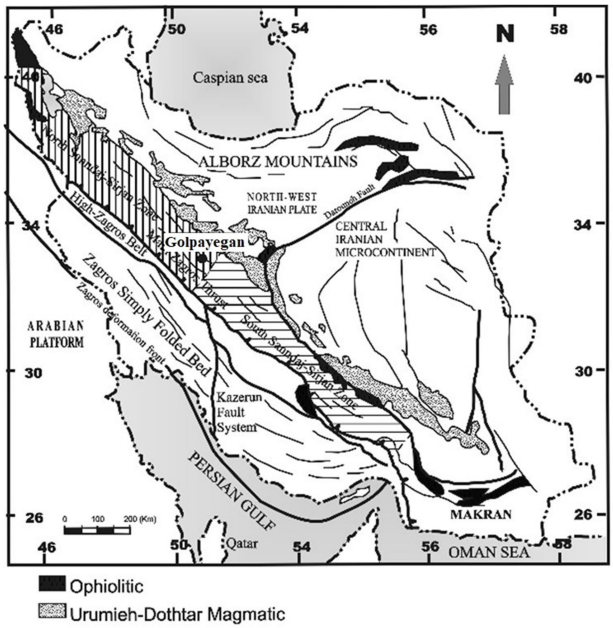


Figure 1: Simplified tectonic map of Iran showing the main structural zones, including the Zagros fold-thrust belt, the Sanandaj-Sirjan Zone (SSZ), and the Urumieh-Dokhtar Magmatic Arc (UDMA). The location of the Golpayegan study area is marked within the central part of the SSZ (modified after Agard et al., 2005).

3. Geology of the Study Area

The oldest exposed rocks in the Golpayegan area are Precambrian metamorphic complexes (gneisses, marbles, amphibolites, schists) (Thiele et al., 1968). Paleozoic sedimentary rocks (sandstones, limestones, shales) and Mesozoic-Cenozoic formations (limestones, marls, sandstones, conglomerates, volcanic rocks) also crop out in the region (Zahedi et al., 1978; Nabavi et al., 1978). This study focuses on the Paleocene-Eocene syenitic magmatic pulse in the northern part of Golpayegan (Fig. 2). Field observations indicate that the syenitic plutonic rocks of northern Golpayegan occur as intrusive bodies with sharp contacts with the surrounding

Mesozoic metamorphic rocks (schists and marbles). The syenites are medium- to coarse-grained, showing a porphyritic texture in hand specimens. They are cross-cut by late-stage mafic dykes, suggesting multiple magmatic pulses. No evidence of significant post-emplacement deformation was observed in the field, although some fractures and minor shear zones are locally present. Previous studies have reported Early Cretaceous ages for some granite, gabbro, and syenite intrusions in northern Golpayegan (Shakerardakani et al., 2020; Moghadam et al., 2024). However, the syenitic rocks investigated here are interpreted as Paleocene-Eocene in age, based on regional geochronological correlations (Rachidnejad-Omran, 2002; Moritz et al., 2006). This age assignment is further supported by their post-collisional tectonic affinity, which is consistent with the Eocene magmatic flare-up documented across Iran (Verdel et al., 2011; Hassanzadeh and Wernicke, 2016). Representative field photographs are provided in Figure 3.

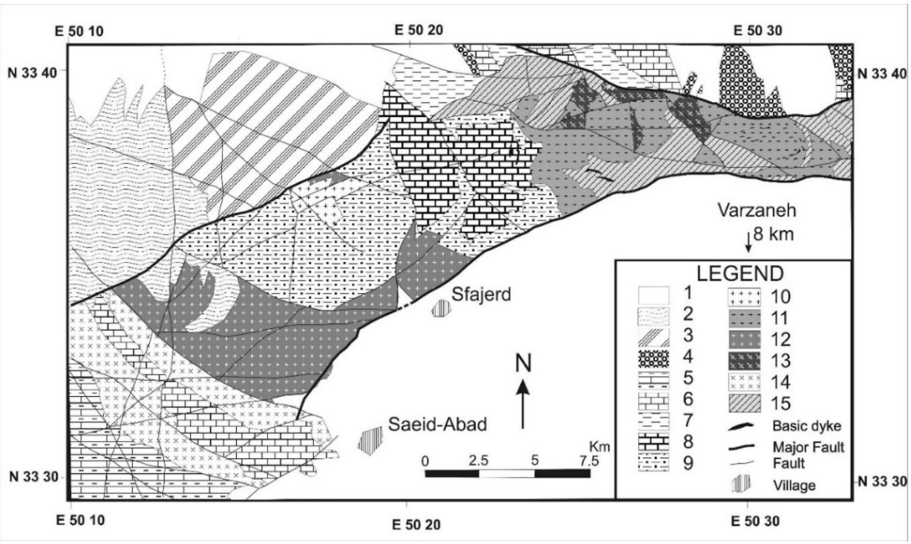


Figure 2: Geological map of the study area, featuring: 1- Recent alluvium, 2- Alluvial terraces, 3- Banding sandstone (Eocene), 4- Sandstone and conglomerate (Eocene), 5- Calcareous shale, Marl, Limestone (Upper Cretaceous), 6- Orbitolina limestone (Lower Cretaceous), 7- Shale (Jurassic), 8- Marble (Mesozoic), 9- Garnet muscovite schist (Mesozoic), 10- Monzogranite (Paleocene), 11- Mylonitic granite (Paleocene), 12- Syenite, Syenodiorite (Paleocene), 13- Mylonitic basic rocks (Middle Jurassic), 14- Trachyte (Cretaceous-Paleocene), and 15- Meta-dacite, Meta-andesite, Meta-rhyolite (Mesozoic).



Figure 3: Representative field photographs of the Golpayegan area: (A) syenitic rocks in contact with Mesozoic Limestone; (B) Trachyte rocks in contact with Mesozoic Limestone.

4. ANALYTICAL METHODS

About 40 rock samples were collected from the Golpayegan area, and only the least altered specimens were selected for petrographic examination. Mineral chemical analyses of amphibole and biotite were conducted using a wavelength-dispersive electron probe microanalyzer (JEOL JXA-8800R) at Naruto University, Japan. The analyses were performed under an accelerating voltage of 15 kV and a beam current of 15 nA. Natural and synthetic minerals of known compositions were used as standards. The standards used for calibration included natural silicates and oxides. Analytical uncertainties for major elements are within ±1–2% relative. Fe^{3+} and Fe^{2+} proportions in amphibole and biotite were calculated using the stoichiometric method of Droop (1987). Although only six biotite grains yielded reliable electron microprobe analyses due to their small grain size and partial alteration in some samples, the consistent compositional trends observed in these data support the interpretations presented in this study.

5. PETROGRAPHY AND MINERAL CHEMISTRY

The studied plutonic rocks are predominantly syenite, as confirmed by total alkalis vs. silica diagram (Le Maitre, 1989; Fig. 4). They exhibit a characteristic porphyritic texture with medium- to coarse-grained crystals. The main mineral components include orthoclase (approximately 80%), amphibole (30–40%), and biotite (1.5–2%). Accessory minerals include titanite (sphene), apatite, tourmaline, and opaque minerals. Some samples show alteration to clay minerals, sericite, chlorite, carbonates, epidote, and magnetite. Plagioclase was not identified in the thin sections; feldspar is exclusively K-feldspar (orthoclase). Biotite occurs as euhedral to subhedral crystals and is the principal mafic phase. Microphotographs illustrating these features are shown in Figure 5.

Representative electron microprobe analyses of biotite and amphibole minerals in the studied plutonic rocks are exhibited in Tables 1 and 2.

Amphiboles are calcic and classified as ferro-tschermakite based on the Fe^{3+}/Al^{6} ratio versus ANa + AK. Biotites are classified as lepidomelane (Fig. 6a, b), with minimal compositional variation.

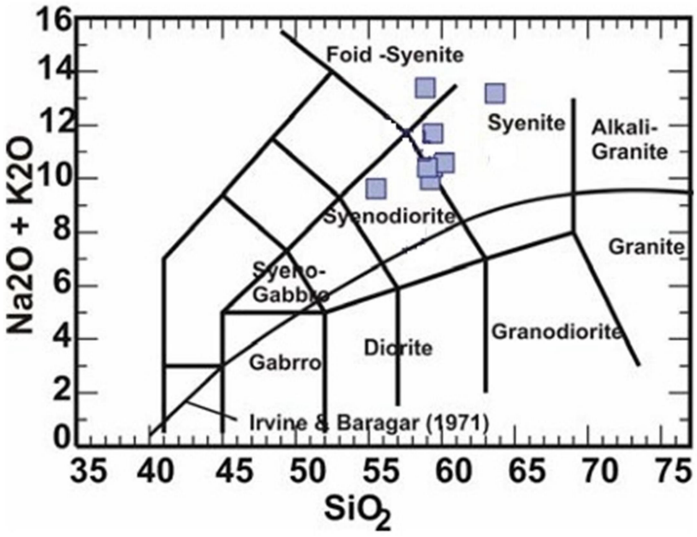


Figure 4: Total alkalis ($Na_2O + K_2O$) versus SiO_2 (TAS) classification diagram for the Golpayegan plutonic rocks (after Le Maitre, 1989). All samples plot within the syenite field, confirming their alkaline affinity.

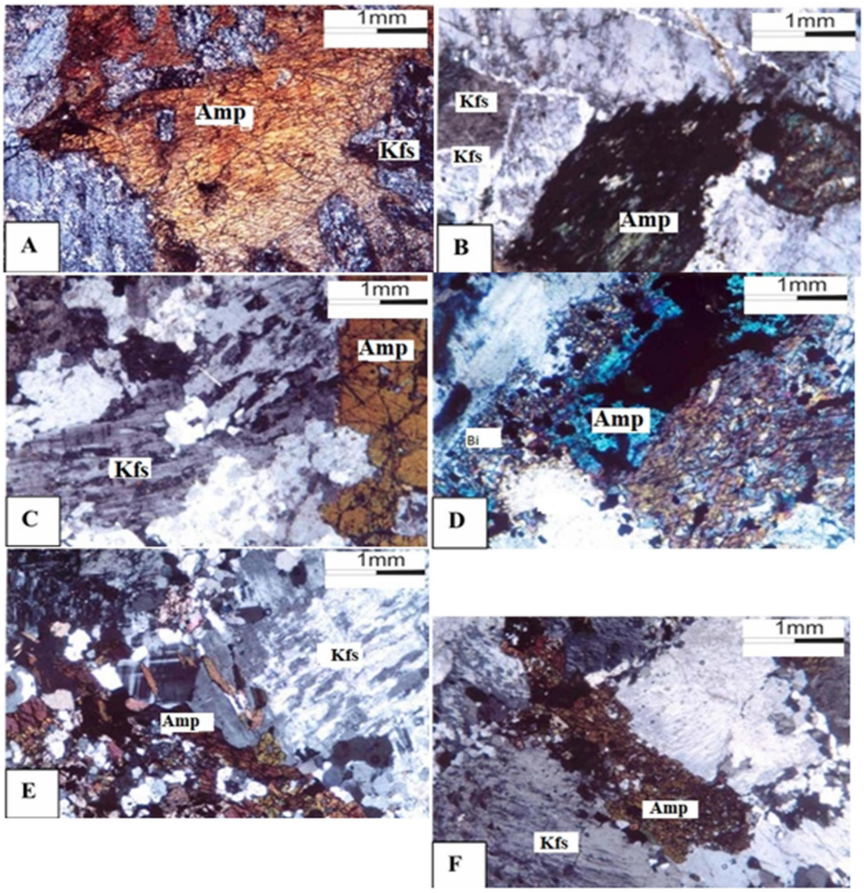


Figure 5. Photomicrographs (crossed-polarized light) of the Golpayegan syenitic rocks. Mineral abbreviations after Kretz (1983). Amp: amphibole; Bi: biotite; Kfs: K-feldspar.

Table 1: Microprobe analyses of biotite phenocrysts from Miocene–Pliocene plutonic rocks located in the north of Golpayegan

	1	2	3	4	5	6
SiO_2	33.84	34.36	33.90	33.84	34.36	33.90
TiO_2	2.87	3.24	3.16	2.87	3.24	3.16
Al_2O_3	14.11	14.22	14.11	14.11	14.22	14.11
FeO	31.60	31.70	32.56	31.60	31.70	32.56
MnO	0.32	0.39	0.41	0.32	0.39	0.41
MgO	2.60	2.71	2.60	2.60	2.706	2.60
CaO	0	0.06	0.00	0	0.06	0.00
Na_2O	0.15	0.16	0.127	0.15	0.16	0.18
K_2O	10.05	10.34	9.58	10.05	10.34	9.58
Li_2O*	0.78	0.75	0.79	0.78	0.75	0.79
TOTAL	96.33	97.93	97.24	96.33	97.93	97.24
Si	2.69	2.69	2.68	2.69	2.69	2.68
Al^{iv}	1.23	1.24	1.25	1.23	1.24	1.25
Al^{vi}	0.09	0.08	0.06	0.09	0.08	0.06
Ti	0.17	0.19	0.19	0.17	0.19	0.19

Fe^{2+}	2.01	1.98	1.95	2.00	1.98	1.95
Fe^{3+}	0.10	0.09	0.20	0.10	0.10	0.20
Mn	0.02	0.03	0.03	0.021	0.03	0.03
Mg	0.31	0.32	0.31	0.31	0.32	0.31
Li*	0.25	0.24	0.25	0.25	0.24	0.25
Ca	0	0.01	8.46	0	0.01	8.46
Na	0.023	0.02	0.02	0.02	0.02	0.02
K	1.02	1.03	0.97	1.02	1.03	0.97
Total	9.96	9.95	9.93	9.96	9.95	9.93
Total T-site	4	4	4	4	4	4
Total M-site	2.95	2.92	2.98	2.95	2.92	2.98
Total I-site	1.04	1.06	0.98	1.04	1.06	0.98
Talc	0.00	0.00	1.55	0.00	0.00	1.55
Ti-Phlogopite	17.98	19.92	19.27	17.98	19.92	19.27
Ferri-Eastonite	10.36	9.91	20.79	10.36	9.91	20.79
Muscovite	0.00	0.00	0.00	0.00	0.00	0.00
Eastonite	9.54	7.86	6.48	9.54	7.86	6.48
Phlogopite	62.12	62.32	51.91	62.12	62.32	51.91

Formulae calculated on the basis of 22 oxygen atoms.

Table 2: Microprobe analyses of amphibole phenocrysts in Paleocene-Eocene plutonic rocks in the north of Golpayeg

Sample number	DK-12-1	DK-12-2	DK-12-3	SF-14-C1	SF-14-C2	SF-14-R1	SF-14-R2	C1-AMP6	C2-AMP1
SiO_2	38.98	38.62	39.40	37.98	37.95	38.02	37.66	40.33	40.24
TiO_2	0.29	0.05	0.05	1.027	0.84	0.70	0.73	0.46	0.14
Al_2O_3	11.23	12.22	12.12	11.24	11.73	12.29	11.75	11.78	12.42
FeO	28.42	28.59	24.56	29.82	28.90	29.46	29.68	22.88	24.18
MnO	1.17	1.28	1.51	0.58	0.54	0.57	0.51	0.33	0.37
MgO	3.36	3.37	6.16	2.075	1.964	1.83	1.97	6.39	5.98
CaO	11.38	11.27	11.75	10.71	10.70	10.75	10.77	10.97	11.05
Na_2O	1.28	1.28	1.35	1.46	1.35	1.27	1.41	1.86	1.88
K_2O	1.77	1.81	1.25	2.37	2.41	2.58	2.41	0.84	0.95
Total	97.88	98.49	98.15	97.25	96.37	97.48	96.88	95.84	97.21
Si	6.16	6.04	6.05	6.14	6.17	6.11	6.10	6.28	6.20
Ti	0.03	0.01	0.01	0.13	0.10	0.08	0.01	0.05	0.02
Al^{iv}	1.84	1.96	1.95	1.87	1.83	1.89	1.90	1.72	1.80
Al^{vi}	0.26	0.30	0.24	0.27	0.42	0.44	0.35	0.44	0.45
Fe^{3+}	0.90	1.12	1.20	0.70	0.55	0.66	0.70	0.78	0.93
Fe^{2+}	2.86	2.62	1.96	3.33	3.37	3.30	3.33	2.19	2.18
Mn	0.16	0.17	0.20	0.08	0.07	0.08	0.07	0.04	0.05
Mg	0.79	0.79	1.41	0.50	0.48	0.44	0.47	1.48	1.37
Ca	1.93	1.89	1.93	1.85	1.86	1.85	1.87	1.83	1.82
Na	0.39	0.39	0.40	0.46	0.43	0.39	0.44	0.56	0.56
K	0.36	0.36	0.24	0.49	0.50	0.53	0.50	0.17	0.19

Formulae calculated on the basis of 23 oxygen atoms.

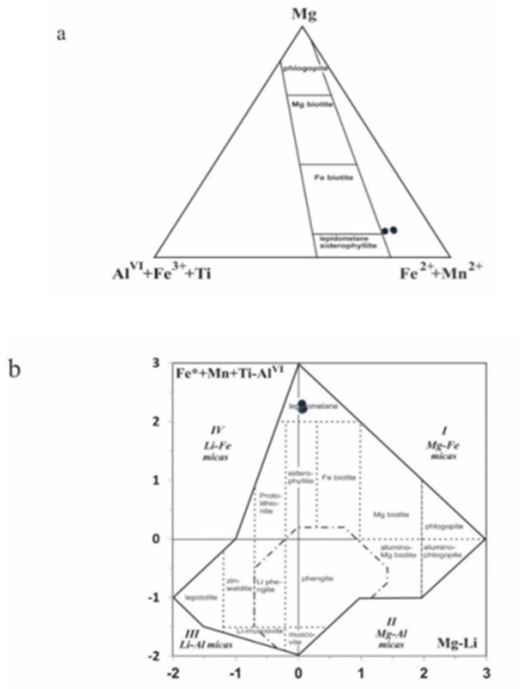


Figure 6: Classification diagrams for biotite from the Golpayegan syenitic rocks: (a) Mg–(AlVI+Fe^{3+}+Ti)–(Fe^{2+}+Mn) ternary diagram (after Foster, 1960a), and (b) Fe/(Fe+Mg) versus Al (after Tischendorf et al., 1997). Both diagrams consistently classify the biotites as lepidomelane, indicating an alkaline magmatic affinity.

6. DISCUSSION

6.1. *Magmatic series*

Biotite chemistry is a reliable indicator of the tectonomagmatic affinity of the parent magma (Abdel-Rahman, 1994). On the Al versus Mg diagram of Nachit et al. (1985) (Fig. 7a), the analyzed biotites plot within the alkaline field. Additionally, on the Abdel-Rahman (1994) discrimination diagrams (Fig. 7b–e), all biotites plot predominantly within the alkaline field. These results indicate that the magma from which the Golpayegan biotites crystallized had an alkaline affinity.

To further confirm the magmatic series, whole-rock geochemical data (Supplementary Table 1) were plotted on a TAS diagram (Fig. 4) and a K_2O vs. SiO_2 diagram (Fig. 8). The samples consistently fall in the syenite field and show alkaline to shoshonitic affinities, which are in good agreement with the biotite-based discrimination. This supports an alkaline magmatic series for the Golpayegan plutonic rocks.

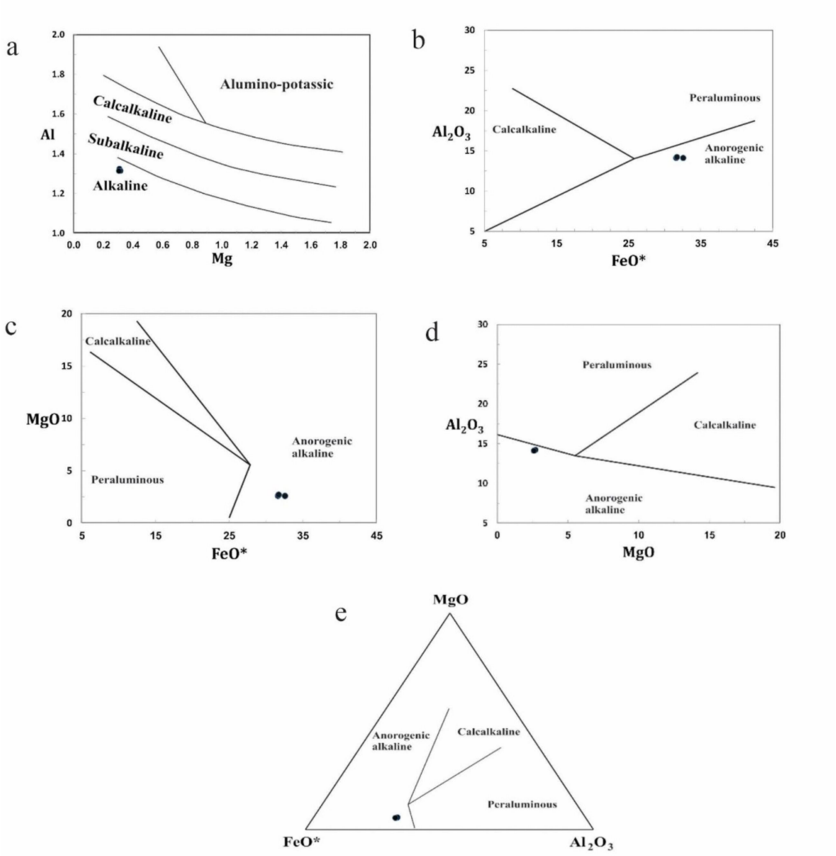


Figure 7: Biotite-based discrimination diagrams for magmatic series identification: (a) Al versus Mg diagram (after Nachit et al., 1985); (b–e) various discrimination diagrams (after Abdel-Rahman, 1994). The analyzed biotites consistently plot within the alkaline field, indicating an alkaline nature for the parental magma.

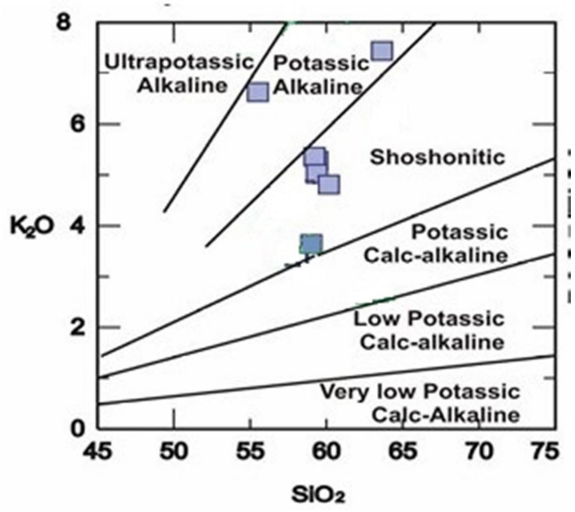


Figure 8: K_2O versus SiO_2 classification diagram for the Golpayegan plutonic rocks (after Maury, 1993). The samples show alkaline to shoshonitic affinities, which is consistent with the alkaline series indicated by biotite chemistry.

6.2. ***Estimate of temperature and pressure***

Geothermobarometric calibrations are widely applied in petrology to constrain the temperature and pressure of mineral crystallization (e.g., Spear, 1995; Ottonello, 1997). Temperature and pressure were estimated using the amphibole-only thermobarometer of Ridolfi et al. (2010) (Table 3). The results indicate that amphibole crystals formed at temperatures of 882–915 °C (average 902 °C) and pressures of 3.68–5.59 kbar (average 4.67 kbar). This pressure range corresponds to a crystallization depth of approximately 15–18 km, indicating emplacement at mid-crustal levels.

The estimated depth of 15–18 km suggests that the Golpayegan syenitic magma crystallized at mid-crustal levels. This is consistent with an post-collisional extensional setting where magma ascent is facilitated by crustal-scale faults. The mid-crustal emplacement, argues favors a model of lithospheric extension or delamination following the main phase of Neo-Tethyan subduction, possibly related to the Eocene magmatic flare-up observed across Iran (Verdel et al., 2011).

6.3. ***Estimation of oxygen fugacity***

The oxygen fugacity of the magma was estimated using the composition of biotite and the Fe^{3+}–Fe^{2+}–Mg diagram of Wones and Eugster (1965) (Fig. 9a). The biotite compositions plot close to the FMQ (Fayalite-Magnetite-Quartz) buffer curve. Using the FMQ buffer equation (Chou, 1978) and the estimated crystallization temperature range of 750–800 °C, a log fO_2 of approximately -13 was calculated (Fig. 9b). This value is consistent with the oxygen fugacity reported for other intermediate to felsic magmas (Carmichael, 1991) and suggests relatively reducing conditions during crystallization.

The relatively low oxygen fugacity (near FMQ) is characteristic of alkaline magmas derived from enriched lithospheric mantle sources, further supporting an post-orogenic extensional setting.

Table 3: Results of amphibole only thermobarometer of Paleocene-Eocene plutonic rocks in the north of Golpayegan

Sample	DK-12-1	DK-12-2	DK-12-3	SF-14-C1	SF-14-C2	SF-14-R1	SF-14-R2	C1-AMP6	C2-AMP1
T	913	911	915	910	909	886	883	887	895
P	4.91	3.90	4.49	4.16	4.87	5.46	4.84	4.30	4.91

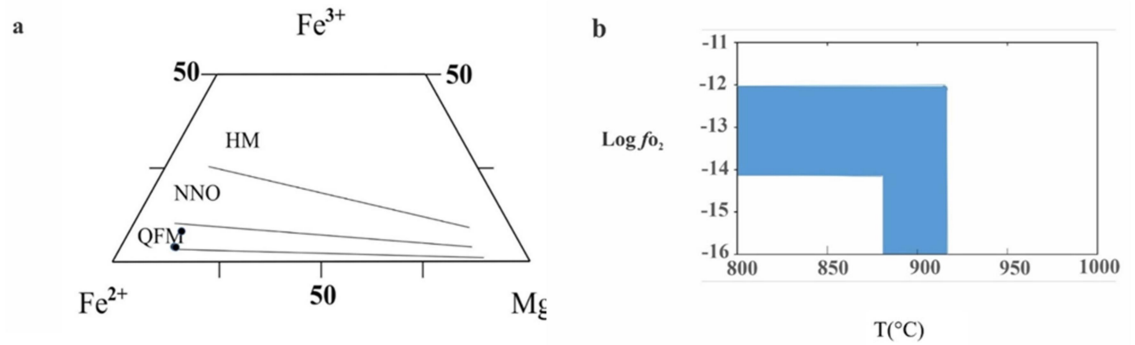


Figure 9: (a) Fe^{2+}–Fe^{3+}–Mg ternary diagram (after Wones and Eugster, 1965) showing the compositions of analyzed biotites relative to the FMQ (fayalite–magnetite–quartz) buffer. (b) Oxygen fugacity (log fO_2) versus temperature diagram, with the FMQ buffer curve calculated using the equation of Chou (1978) for the temperature range 700–900 °C. The estimated log fO_2 value of approximately -13 indicates relatively reducing conditions during biotite crystallization.

Tectonic Setting

Based on the widely used classification of Thompson and Fowler (1986), potassic and ultrapotassic magmas are divided into three tectonic groups: subduction-related, post-collisional, and intracontinental extensional. The potassic magma investigated in the present study clearly falls within the post-collisional group, consistent with formation following the Neo-Tethys closure (Fig. 10). This interpretation is further supported by the classifications of Joplin (1968), Morrison (1980), and Müller et al. (1992), which also correlate the studied rocks with post-collisional arc potassic magmas (Fig. 11a, b). Comparable examples are documented in the Eastern and Western Alps, where continental collision occurred during the Eocene following prolonged subduction (Venturelli et al., 1984; Müller et al., 1992).

In the Sanandaj-Sirjan Zone, the continental crust has been thickened to approximately 60 km, with a low-velocity layer inferred at mid-crustal depths (~30 km; Giese et al., 1984). These findings are interpreted as evidence for the overthrusting of the Iranian crust over the Arabian plate. The region experienced highly complex subduction-related magmatism, and following crustal thickening, the suture zone was subsequently characterized by post-collisional alkaline magmatic activity and tectonic uplift (Wilson, 1989). This is consistent with Best (2003), who linked alkaline magma genesis to regions with thick lithosphere.

Numerous studies on the Sanandaj-Sirjan Zone support a multi-stage tectonic evolution involving the opening, spreading, subduction, and eventual collision and closure of Neo-Tethys (Mohajjel, 1997; Mohajjel & Fergusson, 2000). According to Middlemost (1985), crustal extension and rifting may occur adjacent to active continental margins and collision zones, activating deep-seated faults. The study area, situated along the Africa-Eurasia collision line and the Alpine-Himalayan belt, shares a geological history similar to other Alpine regions, where multiple subduction episodes preceded the final collision (Boccaletti & Guazzone, 1974; Adamia et al., 1980).

Given that the syenites of northern Golpayegan range in age from Paleocene (Rachidnejad-Omran, 2002) to Eocene (Moritz et al., 2006), and the Laramide orogenic phase in Iran is constrained to the post-Upper Cretaceous (Maastrichtian) to pre-Paleocene interval (Allègre & Vialon, 1977; Tillman et al., 1981), it is plausible that these rocks formed after the Laramide phase and are of post-collisional arc potassic type. From a geodynamic perspective, following the Laramide phase, compressional stresses decreased and were replaced by local extensional stresses, leading to deep fracturing and the ascent of mantle-derived basic magma into the crust (Fig. 12).

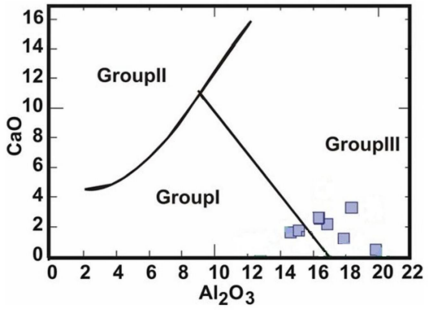


Figure 10: Al_2O_3 versus CaO discrimination diagram for potassic and ultrapotassic magmas (after Thompson and Fowler, 1986). The Golpayegan samples plot in Group III consistent with a post-collisional tectonic setting. Abbreviations: Group I = Continental Collision Zones; Group II = Continental Rift Zones; Group III = Post-Collisional Zones.

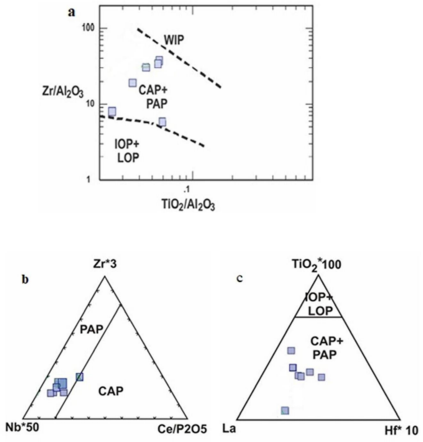


Figure 11: Tectonic discrimination diagrams for the Golpayegan potassic rocks: (a) Zr versus Y diagram (after Müller et al., 1992); (b) Zr/TiO_2 versus Ce/P_2O_5 diagram (after Müller et al., 1992). The studied samples plot predominantly in the post-collisional arc (PAP) field, supporting a post-orogenic origin. Abbreviations: WIP = within-plate; CAP = continental arc; PAP = post-collisional arc; LOP = late-orogenic potassic; MORB = mid-ocean ridge basalt; OIB = ocean island basalt.

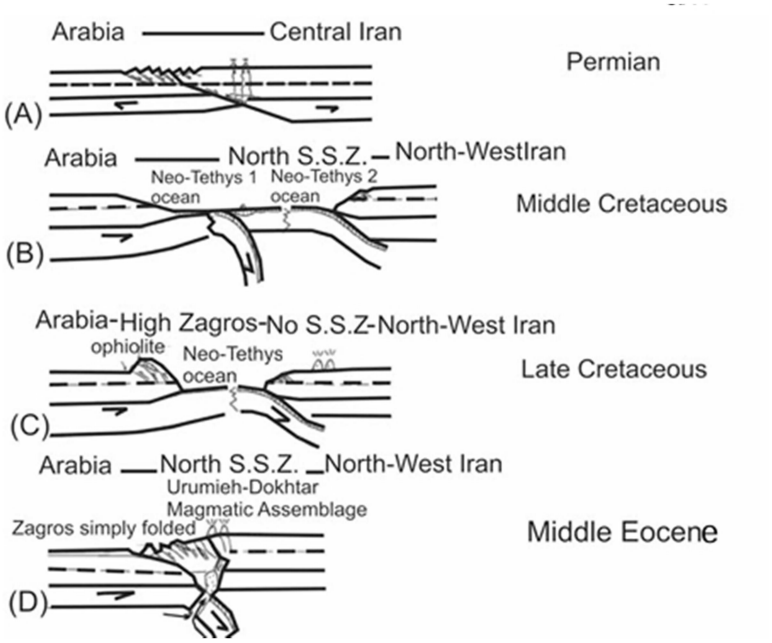


Figure 12: Schematic geodynamic model illustrating the Paleocene-Eocene tectonic evolution of the central Sanandaj-Sirjan Zone and the emplacement of the Golpayegan syenitic plutons (modified after Ghasemi and Talbot, 2006; Agard et al., 2005): (a) northeastward subduction of the Neo-Tethyan oceanic lithosphere beneath the Iranian plate; (b) continental collision and crustal thickening following ocean closure; (c) slab break-off and initiation of post-collisional extension; (d) ascent of alkaline magmas along deep-seated extensional faults, resulting in syenite emplacement at mid-crustal levels (~15–18 km). Abbreviations: SSZ = Sanandaj-Sirjan Zone; UDMA = Urumieh-Dokhtar Magmatic Arc; MZT = Main Zagros Thrust.

7. CONCLUSION

Petrological, mineral chemical, and thermobarometric investigations of the syenitic rocks from northern Golpayegan indicate crystallization from an alkaline magmatic series, with amphiboles classified as ferro-tschermakite and biotites as lepidomelane, displaying limited compositional variation. Amphibole-only thermobarometry yields crystallization temperatures of 882–915 °C and pressures of 3.68–5.59 kbar, corresponding to mid-crustal emplacement depths of approximately 15–18 km. Oxygen fugacity calculations based on biotite composition yield a log fO_2 of approximately -13, indicating relatively reducing conditions near the FMQ buffer, consistent with alkaline magmas derived from enriched lithospheric mantle sources. These results represent the first quantitative P–T–fO_2 estimates for Paleocene-Eocene magmatism in this part of the SSZ.

According to the classifications of Thompson and Fowler (1986), Joplin (1968), Morrison (1980), and Müller et al. (1992), the potassic magmatism in the study area is comparable to post-collisional potassic suites. The Laramide orogenic phase, which occurred after the Late Cretaceous and before the Paleocene, marked a significant transition in the stress regime. Following this phase, compressional stresses diminished and were progressively replaced by local extensional stresses, which facilitated deep-seated fracturing and the ascent of mantle-derived basic melts into the continental crust. This post-collisional alkaline magmatism is analogous to that observed in other segments of the Alpine-Himalayan orogenic belt, such as the Eastern and Western Alps, where complex subduction and collision histories have been documented.

The thickened lithosphere (~60 km) of the Sanandaj-Sirjan Zone, resulting from crustal overthrusting, facilitated alkaline magma generation (Best, 2003). The Paleocene-Eocene syenites of northern Golpayegan are thus post-collisional products of extensional fracturing after the Laramide orogeny and Neo-Tethys closure, representing a local expression of the Eocene Iranian flare-up and constraining the Cenozoic tectonomagmatic evolution of the central Sanandaj-Sirjan Zone.

Acknowledgments

The authors are sincerely grateful to the Earth Science Laboratory in the Naruto University, Japan who made possible the sample preparation and Microprobe analyses. We are really thankful to the Office of Graduate Studies of the University of Isfahan for its support.

REFERENCES

Abdel-Rahman, A. (1994) Nature of biotites from alkaline, calc-alkaline and peraluminous magmas. *Journal of Petrology*, 35, 525–541.

Adamia, S.A., Chkhotua, T., Kekelia, M., Lordkipanidze, M. and Zakariadze, G. (1980) Tectonics of the Caucasus and adjoining regions: implications for the evolution of the Tethys. *Journal of Structural Geology*, 3, 437–447.

Agard, P., Omrani, J., Jolivet, L. and Mouthereau, F. (2005) Convergence history across Zagros (Iran): constraints from collisional and earlier deformation. *International Journal of Earth Sciences*, 94, 401–419.

Allègre, C.J. and Vialon, P. (1977) Structure and evolution of the Zagros Mountains. In: Smith, H.T.U. (Ed.) *Proceedings of the Symposium on the Geodynamics of the Zagros and Central Iran*. Tehran: Geological Survey of Iran, pp. 56–75.

Anderson, J.L. and Smith, D.R. (1995) The effects of temperature and fO_2 on the Al in hornblende barometer. *American Mineralogist*, 80, 549–559.

Berberian, M. and King, G.C.P. (1981) Towards a paleogeography and tectonic evolution of Iran. *Canadian Journal of Earth Sciences*, 18, 210–265.

Best, M.G. (2003) *Igneous and Metamorphic Petrology* (2nd ed.). Blackwell Science.

Boccaletti, M. and Guazzone, G. (1974) Remnant arcs and marginal basins in the Cainozoic development of the Mediterranean. *Nature*, 252, 18–21.

Carmichael, I.S.E. (1991) The redox states of basic and silicic magmas: a reflection of their source. *Contributions to Mineralogy and Petrology*, 106, 129.

Chou, I.M. (1978) Calibration of oxygen buffers at elevated P and T using the hydrogen fugacity sensor. *American Mineralogist*, 63, 690–703.

Droop, G.T.R. (1987) A general equation for estimating Fe^{3+} concentrations in ferromagnesian silicates and oxides from microprobe analyses, using stoichiometric criteria. *Mineralogical Magazine*, 51, 431–435.

Foster, M.D. (1960a) Layer charge relations in the dioctahedral and trioctahedral micas. *American Mineralogist*, 45, 383–398.

Ghasemi, A. and Talbot, C.J. (2006) A new tectonic scenario for the Sanandaj-Sirjan zone (Iran). *Journal of Asian Earth Sciences*, 26, 683–693.

Giese, P., Makris, J. and Riahi, M.A. (1984) Seismic crustal structure of the Zagros Mountains and the Iranian Plateau. In: Gupta, H.K. (Ed.) *Seismic Exploration of the Earth's Crust*. Berlin: Springer-Verlag, pp. 45–58.

Hammarstrom, J.M. and Zen, E. (1986) Aluminum in hornblende: an empirical igneous geobarometer. *American Mineralogist*, 71, 1297–1313.

Hassanzadeh, J. and Wernicke, B.P. (2016) The Neotethyan Sanandaj-Sirjan zone of Iran as an archetype for passive-margin-arc transitions. *Tectonics*, 35, 586–610.

Joplin, G.A. (1968) The shoshonite association: a review. *Journal of the Geological Society of Australia*, 15, 275–294.

Kretz, R. (1983) Symbols for rock-forming minerals. *American Mineralogist*, 68, 277–279.

Le Maitre, R.W. (1989) *A Classification of Igneous Rocks and Glossary of Terms*. Blackwell Scientific Publications.

Maury, R.C. (1993) Les series volcaniques. *Mémoire de la Société Géologique de France*, 163, 39–55.

Middlemost, E.A.K. (1985) *Magmas and Magmatic Rocks: An Introduction to Igneous Petrology*. Longman.

Moghadam, H.S., Li, Q.L., Griffin, W.L., Chiaradia, M. and O'Reilly, S.Y. (2024) Early Cretaceous magmatism in the Sanandaj-Sirjan Zone, Iran: implications for the tectonic evolution of the Neo-Tethys. *Lithos*, 468–469, 107485.

Mohajjel, M. (1997) Structure and tectonic evolution of the Sanandaj-Sirjan zone, western Iran. Unpublished PhD thesis, University of Wollongong.

Mohajjel, M. and Fergusson, C.L. (2000) Dextral transpression in the Sanandaj-Sirjan Zone, Iran. *Journal of Structural Geology*, 22, 1329–1342.

Moritz, R., Ghazban, F. and Singer, B.S. (2006) Eocene gold ore formation at Muteh, Sanandaj-Sirjan tectonic zone, Western Iran: a result of late-stage extension and exhumation of metamorphic basement rocks within the Zagros Orogen. *Economic Geology*, 101, 1497–1524.

Morrison, G.W. (1980) Characteristics and tectonic setting of the shoshonite rock association. *Lithos*, 13, 97–108.

Müller, D., Rock, N.M.S. and Groves, D.I. (1992) Geochemical discrimination between shoshonitic and potassic volcanic rocks from different tectonic settings: a pilot study. *Mineralogy and Petrology*, 46, 259–289.

Nabavi, M.H., Amidi, M., Alavi Tehrani, N., Davoudzadeh, M., Valeh, N. and Aghanabati, A. (1978) *Geological Map of the Nain*. Scale 1:250,000. Geological Survey of Iran.

Nachit, H., Razafimahefa, N., Stussi, J.M. and Carron, J.P. (1985) Composition chimique des biotites et typologie magmatique des granitoides. *Comptes Rendus de l'Académie des Sciences de Paris*, 301, 813–819.

Nouri, F., Azizi, H., Asahara, Y. and Tsuboi, M. (2023) Continental rifting and alkaline magmatism in the Sanandaj-Sirjan Zone, Iran. *Journal of Asian Earth Sciences*, 245, 105559.

Ottonello, G. (1997) *Principles of Geochemistry*. Columbia University Press.

Pirouz, M., Avouac, J.P., Gualandi, A., Hassanzadeh, J. and Sternai, P. (2017) Flexural bending of the Zagros foreland basin. *Geophysical Journal International*, 210, 1659–1680.

Rachidnejad-Omran, N. (2002) Petrology and geochemistry of meta volcano-sedimentary and plutonic rocks of Muteh area with special respect to genesis of gold mineralization, south Delijan, SSW of Tehran, Iran. PhD Thesis, University of Tarbiat Modares, Tabriz, 420 p.

Ridolfi, F., Renzulli, A. and Puerini, M. (2010) Stability and chemical equilibrium of amphibole in calc-alkaline magmas: an overview, new thermobarometric

formulations and application to subduction-related volcanoes. *Contributions to Mineralogy and Petrology*, 160, 45–66.

Schmidt, M.W. (1992) Amphibole composition in tonalite as a function of pressure: an experimental calibration of the Al-in-hornblende barometer. *Contributions to Mineralogy and Petrology*, 110, 304–310.

Shakerardakani, F., Neubauer, F., Bernroider, M. and Friedl, G. (2020) Early Cretaceous magmatism in the Sanandaj-Sirjan Zone, Iran: geochronology, geochemistry, and tectonic implications. *International Journal of Earth Sciences*, 109, 161–183.

Sharifi, M. (2007) Investigation of Alkaline Magmatism in the North of Golpayegan Area. PhD thesis, University of Isfahan, Isfahan (in Persian).

Spear, F.S. (1995) *Metamorphic Phase Equilibria and Pressure-Temperature-Time Paths*. Mineralogical Society of America.

Thiele, O., Alavi, M., Assefi, R., Hushmand-Zadeh, A., Seyed-Emami, K. and Zahedi, M. (1968) *Popayan Quadrangle Map (1:250,000) with Explanatory Text*. Geological Survey of Iran.

Thompson, R.N. and Fowler, M.B. (1986) Subduction-related shoshonitic and ultrapotassic magmatism: a study of the Oligocene and Miocene volcanic rocks of the Western Alps. In: Fitton, J.D. and Upton, B.G.J. (Eds.) *Alkaline Igneous Rocks*. Geological Society of London, Special Publication No. 30, pp. 253–267.

Tillman, J.E., Poosti, A., Rossello, S. and Eckert, A. (1981) Structural evolution of Sanandaj-Sirjan ranges near Esfahan, Iran. *AAPG Bulletin*, 65, 674–687.

Tischendorf, G., Gottesmann, B., Förster, H.J. and Trumbull, R.B. (1997) On Li-bearing micas: estimating Li from electron microprobe analyses and improved diagram for graphical representation. *Mineralogical Magazine*, 61, 809–834.

Verdel, C., Wernicke, B.P., Hassanzadeh, J. and Guest, B. (2011) A Paleogene extensional arc flare-up in Iran. *Tectonics*, 30, TC3008.

Wilson, M. (1989) *Igneous Petrogenesis: A Global Tectonic Approach*. Unwin Hyman.

Wones, D.R. and Eugster, H.P. (1965) Stability of biotite: experiment, theory, and application. *American Mineralogist*, 50, 1228–1272.

Zahedi, M., Samadian, M., Taavosian, Sh. and Amidi, M. (1978) *Geological Map of the Isfahan*. Scale 1:250,000. Geological Survey of Iran.